Enantioselective optical forces in gain-functionalized single core-shell chiral nanoparticles

R. Ali,[1,*] F. A. Pinheiro,[2] R. S. Dutra,[3] T. P. Mayer Alegre,[1] and G. S. Wiederhecker[1,†]

[1]*Applied Physics Department, Gleb Wataghin Physics Institute, University of Campinas, Campinas 13083-859, São Paulo, Brazil*

[2]*Instituto de Física, Universidade Federal do Rio de Janeiro, Caixa Postal 68528, Rio de Janeiro, Rio de Janeiro 21941-972, Brazil*

[3]*LISComp-IFRJ, Instituto Federal de Educação, Ciência e Tecnologia, Rua Sebastião de Lacerda, Paracambi, Rio de Janeiro 26600-000, Brazil*

(Received 18 April 2023; accepted 5 September 2023; published 9 October 2023)

We propose a gain-assisted enantioselective scheme in dye-doped chiral particles, demonstrating optical pulling and pushing forces that can be tuned using externally controllable parameters. By controlling the concentration of dye molecules and the pumping rate, we achieve all-optical chiral resolution of racemic mixtures and enantioselection of small dipolar chiral particles without relying on interference. This scheme is applicable to both lossless and lossy plasmonic chiral particles, making it a promising approach for chiral sensing, drug discovery, and molecular separation.

DOI: 10.1103/PhysRevA.108.043704

I. INTRODUCTION

An object is said to be chiral if it has distinguishable mirror images; these two opposite mirrored forms are called enantiomers [1–5]. The separation of chiral enantiomers is an important scientific and technological task with many multidisciplinary applications [6,7]. In the last few decades, considerable effort and progress have been made on the development of highly efficient optical enantioselective methods, such as enantioselective optical trapping [8–11], repulsive transverse forces [12–19], enantioselective pulling forces [20,21], and azimuthal and longitudinal optical torques [22,23]. Chiral optical forces, including applications to enantioselection and the possibility of achieving pulling forces using chirality, have also been extensively investigated [9,18,20,24–27]. Despite the rich literature on optical enantioselective schemes, in many cases they involve optical trapping of lossless particles using structured or tightly focused optical beams [8,28–33]. Enantioselection may also be achieved by exploiting transversal forces without strictly relying on scattering forces using lossy chiral spheres, where transversal forces can actually cause repulsion of chiral enantiomers [16,17]. However, enantioselection based on axial forces of lossy chiral particles with an arbitrary degree of absorption remains challenging and restricted due to the weak restoring force.

This restriction occurs because optical trapping and pulling forces rely on the relative strength between optical restoring (coming from the intensity gradient or interface between the incident and scattered fields) and scattering forces (coming from the optical scattering). When considering more general lossy particles, such force competition strongly depends on both absorption level and particle size. As a result, regardless of the particle size, enantioselection becomes difficult due to strong pushing forces, which increase with absorption. In addition, in the case of a dipolar chiral particle with a negligibly small magnetic dipole, the interface between the dipoles is small; therefore, the realization of the pulling effect is impossible due to the lack of a restoring force.

To circumvent these limitations, we propose an alternative strategy that simultaneously enables chiral separation and long-range optical manipulation of a single chiral sphere. We consider an optical gain-functionalized chiral sphere, which enables one to exert tunable optical pulling and pushing forces using a single circularly polarized (CP) plane wave. The main advantage of using gain is to eliminate the dependence on interference to achieve the restoring forces, in contrast to existing enantioselective methods based on optical forces [12,13,19,20,34]. Here, restoring force is achieved through the emission of photons due to gain mechanisms, and the number of emitted photons increases with the active size of the sphere. As the optical gain can be experimentally controlled with great success, it allows us to exert the necessary tunable optical pulling and pushing forces on demand. This work is intended to carry out a detailed study of the enantioselection of chiral Mie spheres and chiral dipoles by employing experimentally controllable parameters such as the laser pump rate of the dye molecules.

To accomplish this study, first, we consider a chiral core-shell particle to establish the underlying physics and connection between the gain mechanism and optical forces. Further, we explore the enantioselection of the chiral particles using experimentally achievable parameters. After establishing the enantioselection with the gain media we check the viability and robustness of this scheme by discussing the optical forces acting on the homogeneous chiral sphere and chiral dipoles. In addition, we also show that our scheme can perform enantioselection of the chiral molecules with arbitrarily small chiral parameters and small sizes.

II. RESULTS AND DISCUSSION

A. Optical force on the dielectric core and chiral shell particle

To begin with, we consider chiral core-shell spheres to calculate the chiral and optical gain-dependent forces. This

*rali.physicist@gmail.com
†gsw@unicamp.br

model is general enough to describe a wide range of chiral nanoparticles of scientific and technological interest, such as gain-doped chiral nanocrystals [35], and core-shell particles with a dielectric core and a plasmonic shell [22,36–39]. For the sake of generality (in the latter part of the paper, See II B) we consider the case of a single homogeneous chiral sphere doped with gain, a model that can be applied to gain-doped chiral nanocrystals [35]. To this end let us consider a CP plane wave $\mathbf{E} = E_0(\hat{x} + i\sigma\hat{y})e^{ikz}$ [$\sigma = +1$ (-1) is the spin index of a left- (right-) handed CP plane wave] impinging on particles made of the dielectric core (with radius b and relative permittivity $\epsilon_{\rm d}$) and a chiral shell of thickness t and refractive index $n_\sigma = \epsilon_s + \sigma\kappa$, where ϵ_s is relative permittivity and κ is the chiral index, immersed in water with relative permittivity $\epsilon_w = 1.77$. The optical force acting on the sphere due to a plane wave (see Appendix C) is written in terms of scattering efficiency $Q_{\rm s}$ and absorption efficiency $Q_{\rm a}$ (see Appendix B) as [40]

$$F = \frac{\epsilon_0\epsilon_w E_0^2}{k_w^2}[Q_{\rm a} + Q_{\rm s}(1 - \langle\cos\theta\rangle)] = F_{\rm a} + F_{\rm s}, \qquad (1)$$

where E_0 is the electric-field amplitude, ϵ_0 is the vacuum permittivity, k_w is a wave vector inside the surrounding medium, and $\langle\cos\theta\rangle \equiv g$ is the scattering asymmetry parameter [40] (θ is the scattering angle). The total force can be divided into two force contributions: scattering force $F_{\rm s}$ and absorption force $F_{\rm a}$ [40]. It is clear from Eq. (1) that for a passive chiral sphere, where $\{Q_a, Q_s\} \geqslant 0$, $-1 \leqslant g \leqslant 1$, and $\{F_a, F_s\} \geqslant 0$, the optical force F is always positive, regardless of the chiral handedness, in which case chiral resolution impossible.

However, in the presence of the gain media, the momentum of stimulated emission photons may be strong, and one may expect $F_{\rm s} > 0$ and $F_{\rm a} < 0$; hence a fine tuning of the gain level allows us to control the direction of F on each chiral face, as indicated in Figs. 1(a) and 1(b). For instance, for a passive particle [Fig. 1(a)], the momentum of the scattered photon $\mathbf{P}_s$ can never be larger than the momentum of the incident photon $\mathbf{P}_i$ (i.e., $\mathbf{P}_i - \mathbf{P}_s \geqslant 0$). Therefore, the momentum transfer to the particle should lead to a net positive (pushing) force. In contrast, in an active particle with sufficient gain [Fig. 1(b)], F_a may have its sign reversed because it may be dominated by the recoil from stimulated emission photons with momentum $\mathbf{P}_e$ [41,42], inducing a negative (pulling) force F_a, as illustrated in Fig. 1(b). Since the shell is chiral, in addition to the gain-enabled pulling force $F_{\rm a} < 0$, the particle refractive index depends on the incident-field helicity, which leads to a distinct scattering efficiency Q_s for each enantiomer. Therefore, the gain-tunable pulling force—associated with the chiral-sensitive pushing scattering force—is the key mechanism underlying our tunable enantioselection scheme. Note that our enantioselective scheme involves two laser sources, namely, the probe and the pump beams, indicated by black and purple arrows in Fig. 1(b), respectively. However, it is worth mentioning that we take into account only the radiation pressure coming from the probe beam in Eq. (1), and the force contribution coming from the pump laser can be neglected due to its normal orientation relative to the incident laser axis [42].

We quantitatively demonstrate the effectiveness of our enantioselection scheme by considering a passive core

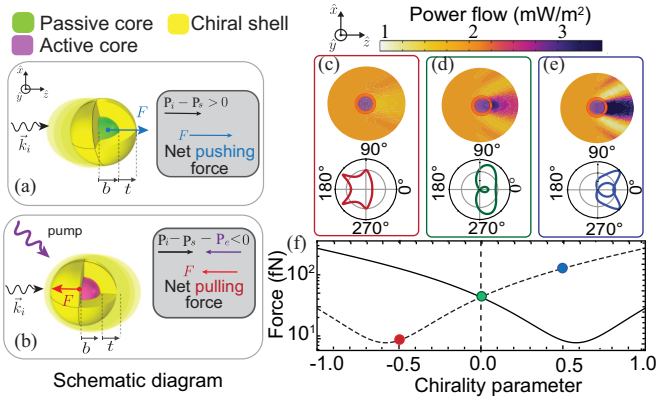

FIG. 1. Schematic of optical forces on the sphere: (a) a CP plane-wave scattering by core-shell, passive-core, and chiral-shell particles, where $\mathbf{P}_i$ and $\mathbf{P}_s$ are the momenta of the incident and scattered photons. The resultant net optical force on the sphere is pushing $F \geqslant 0$. (b) The doped core, dye molecules, and pump laser (normal to the incident beam) enable a gain mechanism; as a result, photons are emitted with momentum $\mathbf{P}_e$, and the net optical force on the active chiral core and shell can be negative. Numerically calculated power flow of the relative scattered fields and polar scattering pattern by the passive chiral core and shell for chirality parameter (c) $\kappa = -0.5$, (d) $\kappa = 0$, and (e) $\kappa = 0.5$. (f) The optical force acting on the passive sphere as a function of the chirality parameter for left CP (dashed line) and right CP (solid line).

$(\epsilon = 2.5)$ with radius $b = 200\,\text{nm}$ and chiral shell ($n_\sigma = 1.7 + \sigma\kappa$) with thickness $t = 80\,\text{nm}$ illuminated by a left-CP plane wave. Using COMSOL MULTIPHYSICS, we numerically calculate the power flow of the scattered fields for different chirality parameters $\kappa = -0.5$, $\kappa = 0$, and $\kappa = 0.5$, as shown in Figs. 1(c)–1(e), respectively. The bottom row in Figs. 1(c)–1(e) shows the polar representation of the scattered field. It is clear that the scattered momentum for the left-handed chiral sphere in Fig. 1(e) is larger than that of the right-handed sphere in Fig. 1(c), in agreement with the qualitative arguments above. When particle and beam handedness are opposite (lower refractive index), scattering is minimum, and hence, the pushing optical force is minimized, as shown in Fig 1(f), where the optical force as a function of the chirality is shown for right- (dotted line) and left- (solid line) handed CP incident light. To understand the precise role of the chiral refractive index in the scattering force, we show the scattering efficiency in Fig. 2(a) (left CP incident beam). Indeed, Q_s is very weak at $\kappa = -0.5$, and a stronger Q_s is found for $\kappa = 0.5$. This behavior is also consistent with chiral sphere polarizability α, as shown in Fig. 2(b). The magnitudes of both the real and imaginary parts are minimized at $\kappa = -0.56$, strongly suppressing the scattered radiation and thus revealing the physics underlying the suppression of the scattering force. In contrast, the sphere with opposite chirality, $\kappa = +0.56$, has a large polarizability and hence a large scattering efficiency and pushing force.

So far, the chiral response of our particles is solely influenced by the passive optical properties. We now discuss the impact of the optical gain on optical forces. In Fig. 2(c) we calculate $Q_{\rm ext}(\epsilon'', \kappa)$ [43] and $Q_{\rm s}(\epsilon'', \kappa)$ of the particles as a function of the chirality parameter with fixed real relative

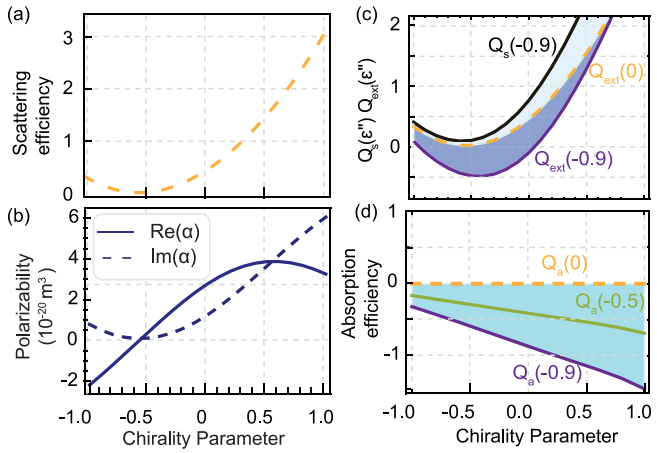

FIG. 2. (a) Scattering efficiency Q_s and (b) total chiral polarizability of the passive chiral sphere as a function of the chirality parameter. (c) Scattering efficiency $Q_s(\epsilon'')$, extinction efficiency $Q_{\text{ext}}(\epsilon'')$, and (d) absorption efficiency versus the chirality parameter $Q_a(\epsilon'')$ for different imaginary permittivities ϵ'' (controlled by the gain parameter); the remaining parameters are the same as in Fig. 1.

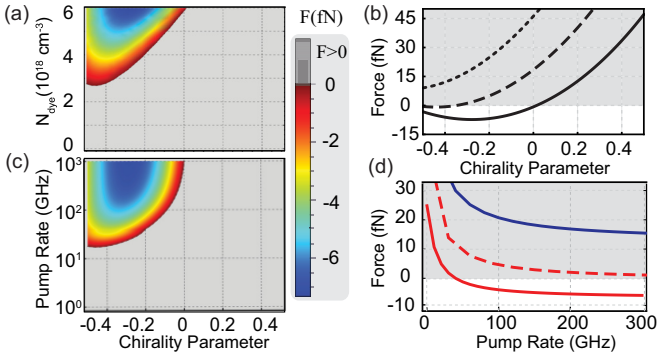

FIG. 3. (a) Net optical force as a function of the chirality parameter and number density N_{dye}. (b) Optical force versus chirality parameter for $N_{\text{dye}} = 0$ (dotted line), $N_{\text{dye}} = 3 \times 10^{18}\,\text{cm}^{-3}$ (dashed line), and $N_{\text{dye}} = 6 \times 10^{18}\,\text{cm}^{-3}$ (solid line). (c) Force-density plot as a function of the chirality parameter and pump rate for fixed $N_{\text{dye}} = 5 \times 10^{18}\,\text{cm}^{-3}$. (d) Optical force as a function of pump rate for different chirality parameters: $\kappa = 0.2$ (blue line), $\kappa = 0$ (red dashed line) and $\kappa = -0.2$ (red solid line). In all calculations $b = 200\,\text{nm}$, $t = 80\,\text{nm}$, $\sigma = -1$, and $\lambda = 1064\,\text{nm}$.

permittivity ϵ_{d} and for different imaginary permittivities ϵ'' of the core, which can be controlled by the pump-induced gain level; the other geometric parameters are the same as in Fig. 2(a). While $Q_{\text{ext}} = Q_{\text{s}}$ for a passive core, this identity does not hold for an active core particle. In this case, the extinction efficiency becomes negative for larger gain for the right-handed chiral sphere [$Q_{\text{ext}}(-0.9, \kappa < 0)$ in Fig. 2(c)]. This difference appears in the absorption efficiency $Q_a(-0.9, \kappa) = Q_{\text{ext}}(-0.9, \kappa) - Q_s(-0.9, \kappa)$. Note that for a lossy sphere extinction efficiency is always less than scattering efficiency, Q_a remains positive, and optical forces on the sphere are pushing forces. However, for the active sphere, the pump rate of the gain medium allows us to achieve negative absorption, and the corresponding optical force becomes a pulling force. Figure 2(d) shows that for larger gain level $Q_a(\epsilon'', \kappa) < 0$ for a broad range of values of κ, so that with Eq. (1) the optical pulling force ($F < 0$) can be achieved.

To ground our study in specific context, we consider a realistic gain model in which the dielectric core is doped with a judicious number of dye molecules [44–46]. For our purpose, we consider the gain properties of solvatochromic LDS 798 dye molecules [44,47,48] in a dielectric ϵ_{d} host, which is a well-established combination to achieve active particles [49,50]. The dye molecules are modeled as four-level atomic systems with occupation number density N_i, and $\sum_0^4 N_i = N_{\text{dye}}$ represents the total number of dye molecules per cubic meter. The effective permittivity of the dye-doped dielectric core is [44–46]

$$\epsilon_g = \epsilon_0\epsilon_{\text{d}} + \frac{\sigma_b N_{\text{dye}}}{\omega^2 + i\Delta\omega_a\omega - \omega_a^2}\frac{(\tau_{21} - \tau_{10})\Gamma_{\text{pump}}}{1 + (\tau_{32} - \tau_{21} + \tau_{10})\Gamma_{\text{pump}}}, \tag{2}$$

where $\sigma_b = \frac{6\pi\epsilon_0 c^3\eta}{\tau_{21}\omega_a^2\sqrt{\epsilon_h}}$, $\omega = 2\pi c/\lambda$, c is the speed of light, $\Delta\omega_a$ is the bandwidth of the dye transition between the two levels resonant with the incident beam, $\omega_a = 2\pi c/\lambda_a$ is the frequency of the emitted photon, $\tau_{i+1,i}$ is the relaxation time between the $(i+1)$th and ith levels, and Γ_{pump} is the pump rate of the dye molecules [44,47]. Equation (2) indicates that the optical gain can be externally controlled by appropriately tuning the emission photons by means of N_{dye} and the pump rate of the dye to activate the gain mechanism. We choose the following parameters to describe the optical gain level given by Eq. (2): $\Delta\omega_a = 175$ THz, $\lambda_a = 777\,\text{nm}$, $\eta = 0.48$, $\tau_{10} = \tau_{32} = 100\,\text{fs}$, and $\tau_{21} = 50\,\text{ps}$ [44,47].

We now demonstrate the tunability of the enantioselection by taking moderate values of dye concentration [51] and experimentally achievable pump power, where dye quenching and the nonlinear effect can be ignored [44,45]. In Fig. 3(a), we compute the optical force acting on a dye-enriched core-shell particle as a function of the chirality parameter and N_{dye} for fixed $\Gamma_{\text{pump}} = 100\,\text{GHz}$. Figure 3(a) shows that optical pulling forces ($F < 0$) gradually vanish as the chirality parameter approaches zero, showing that pulling force is not possible for nonchiral gain-enhanced particles at this dye concentration. Note that higher dye concentrations could lead to a net pulling force even for nonchiral particles ($N_{\text{dye}} > 6 \times 10^{18}\,\text{cm}^{-3}$). Also, the optical force is always pushing ($F > 0$) for passive spheres ($N_{\text{dye}} = 0$), regardless of the chirality parameter. As one increases N_{dye}, the emission photons from the dye molecules in the core also increase, and since the scattering force F_s for the right-handed chiral $\kappa < 0$ particle is weak, there is a critical value, $N_{\text{dye}} \approx 3.2 \times 10^{18}\,\text{cm}^{-3}$, above which right-handed chiral particles experience pulling forces. On the other hand, for left-handed chiral $\kappa > 0$ spheres, the optical force is always pushing ($F > 0$) due to large F_s. This crossover between optical pulling and pushing forces for particles with $\kappa < 0$ shells can also be noticed by inspecting the horizontal linecuts of the density plots in Fig. 3(a), as shown in Fig. 3(b), where F as a function of κ is calculated for increasing dye concentrations $N_{\text{dye}} = \{0, 3, 6\} \times 10^{18}\,\text{cm}^{-3}$ for fixed $\Gamma = 100$ GHz. Interestingly, for $N_{\text{dye}} > 6 \times 10^{18}\,\text{cm}^{-3}$, chiral resolution is achieved for particles in which the shell is made of materials with very small chirality parameters Although the dynamical tuning of the dye concentration in experiments

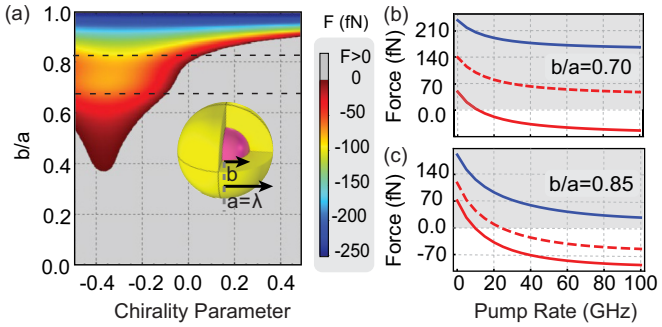

FIG. 4. (a) Density plot representing the optical force as a function of the chirality parameter and the ratio between the core radius b and outer radius $a = b + t = \lambda$ for fixed $\Gamma_{\text{pump}} = 100\,\text{GHz}$ and $N_{\text{dye}} = 5 \times 10^{18}\,\text{cm}^{-3}$. The inset illustrates the particle under consideration. Optical force as a function of pump rate for fixed (b) $b = 0.7a$ and (c) $b = 0.85a$ for different chirality parameters: $\kappa = 0.2$ (blue line), $\kappa = 0$ (red dashed line) and $\kappa = -0.2$ (red solid line). All the other parameters are the same as in (a).

might be difficult, in view of Eq. (2), one can alternatively control the gain level by varying the pump rate at a fixed dye concentration, which is more realistic in practice. This tuning knob is explored in Figs. 3(c) and 3(d); the net optical force is calculated as a function of the chirality parameter and Γ_{pump} for fixed $N_{\text{dye}} = 5 \times 10^{18}\,\text{cm}^{-3}$. The behavior is similar to varying dye concentration; a power threshold exists to achieve pulling forces, provided some degree of chirality is present.

It is worth mentioning that even for low incident intensity, $I_0 = 1\,\text{mW}/\mu\text{m}^2$, the optical pulling force is larger than the Brownian force. In the present study, the Brownian force $F_B \approx 5$ fN (see Appendix A). However, the pulling force can further be improved by increasing the pump rate or incident intensity I_0. To infer the critical pump rate needed to achieve enantioselection, we show in Fig. 3(d) vertical linecuts of Fig. 3(c), revealing the optical force as a function of pumping rate for chirality parameters $\kappa = \{-0.2, 0, +0.2\}$ for fixed $N_{\text{dye}} = 5 \times 10^{18}\,\text{cm}^{-3}$. While the optical force is always positive when $\Gamma_{\text{pump}} = 0$, as the system is excited with an external optical pump, the sign of the net optical force is strongly dependent on the handedness of the chiral shell. In particular, the value of the chirality parameter of the shell defines the threshold pump rate at which the optical force changes sign, a consequence of the amplified photon emission F_a overcoming F_s, which is due to the scattered and radiative losses. This threshold pumping rate can also be estimated from Fig. 4(c).

To demonstrate the robustness of our findings against the geometrical parameters of the core-shell nanostructure, we calculate the optical force as a function of the chirality parameter and the ratio between the core b and outer radii $a = b + t$ in Fig. 4(a). It is worth noting that for a small active core $b/a \ll 1$, where the role of dye molecules is negligible, $F_s \gg F_a$, and therefore, the total optical force is positive. At $b = 0.4a$ the core and shell with $\kappa \approx -0.4$ undergo a pushing to pulling force crossover due to the fact that in this situation the particle is expected to be subjected to weak scattering force F_s; hence, a small emission of photons is sufficient to overcome the scattering force $F_a > F_s$. As a result optical pulling force exists for $\kappa = -0.4$, while pushing forces occur for $\kappa = 0.4$. This result shows that an enantioselective mechanism could be implemented for core-shell spheres with a broad range of geometrical parameters. On the other hand, for $t \gg b$, when the active core is large, the particle is subjected to pulling force regardless of the chirality parameters.

Like in the previous analysis, the threshold pump power required to perform chiral resolution can be more clearly seen by inspecting the force dependence on the pump rate. The robustness of the chiral resolution to geometry fluctuations can be noticed by considering two geometric configurations: $b = 0.7a$ and $b = 0.85a$; the corresponding optical forces, as a function of the pump rate, are plotted in Figs. 4(b) and 4(c), respectively, for different values of the chirality parameter: $\kappa = 0.2$ (blue line), $\kappa = 0.0$ (red dashed line), and $\kappa = -0.2$ (red solid line). From the analysis of Figs. 4(b) and 4(c) we can conclude that right-handed chiral spheres undergo pulling force for a pump rate larger than 10 GHz, despite the fact these two systems have different gain levels and different sizes of the active gain core. In order to understand this result, we should note that the scattering force is smaller in the configuration depicted in Fig. 4(b), which has a thicker chiral shell. As a result, for such a system, weaker light amplification is sufficient to fulfill the condition $|F_a| > |F_s|$ to achieve the net optical pulling force. On the other hand, in comparison to the configuration shown in Fig. 4(c), the shell is thinner, and $|F_s|$ is expected to be larger, but at the same time $|F_a|$ becomes large due to the increased volume of the gain media. This fact compensates the increase in $|F_s|$ for generating a net pulling force in the configuration in Fig. 4(c). Consequently, the overall result is that this configuration exhibits approximately the same critical pump rate (25 GHz), to achieve the pulling forces.

B. Optical pulling force on a homogeneous chiral sphere

In order to improve the generality of this scheme, in this section we discuss optical forces on a gain-functionalized homogeneous chiral sphere, where the chirality is uniform across the particle. This type of chiral sphere may constitute a variety of synthesized chiral examples, such as DNA-assembled nanoparticles, cholesteric liquid crystals, carbon nanotubes, chiral nanocrystals, and chiral quantum dots [3,7]. In addition to the spherical particles, this approach can also be applied to asymmetric or randomly shaped geometrical particles that show large circular dichroism, as shown in [3,35,52]. Without loss of generality, we have added the dye molecules inside the chiral sphere to activate the role of gain media (see details in the previous section). As a continuation of our discussion reported in the Sec. II A, we calculate the optical force acting on the active chiral sphere as a function of the chirality parameter and dye concentration in Fig. 5(a). The results show that even for this configuration we can exert chirality-dependent optical forces on the sphere, which provides an opportunity to perform chiral selection of the homogeneous chiral sphere. For deeper insights, we consider a chiral sphere with an arbitrarily small value of $\kappa = \pm 0.05$ illuminated by a left-handed circularly polarized field to calculate the optical force as a function of pump rate for fixed dye concentration. Figure 5(b) shows that even for small chirality parameters right-handed chiral spheres experience pulling force for incident intensity

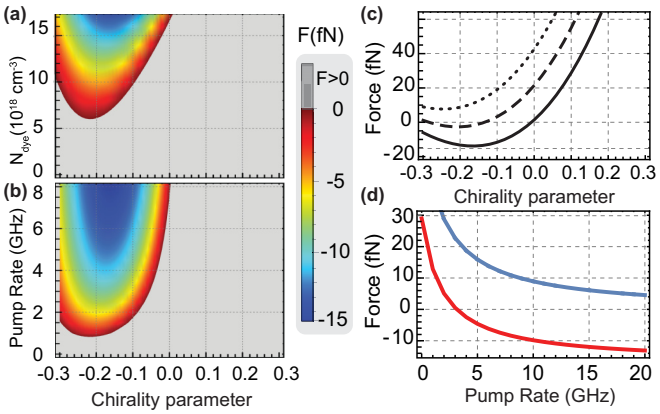

FIG. 5. (a) Optical force acting on a gain-functionalized chiral sphere as a function of the chirality parameter κ and dye concentration for fixed pump rate at 50 GHz. (b) Optical force as a function of the chirality parameter and pumping rate for fixed dye concentration at 1.5×10^{18} cm^{-3}. (c) Optical force versus the chirality parameter for different dye concentrations $N_{\text{dye}} = 0$ (dotted line), $N_{\text{dye}} = 8 \times 10^{18}$ cm^{-3} (dashed line) and $N_{\text{dye}} = 16 \times 10^{18}$ cm^{-3} (solid line), where pumping rate is the same as (a). (d) The optical force acting on a sphere with chirality parameters $\kappa = -5 \times 10^{-2}$ (red line) and $\kappa = 5 \times 10^{-2}$ (blue line) as a function of the pump rate, where dye concentration is fixed at $N = 1.5 \times 10^{18}$ cm^{-3}. This calculation is carried out by taking the refractive index of the sphere $n_s = \sqrt{\epsilon_g} + \sigma\kappa$, where ϵ_g is given in Sec. II A.

$I_0 = 1\,\text{mW}/\mu\text{m}^2$. This confirms that this is a sufficiently large force to overcome the Brownian force. Thus, our scheme is robust against the selection of the chiral structures, and one can perform the chiral resolution of the racemic mixture by controlling the pumping rate of the dye molecules for small values of the chirality parameter.

C. Pulling force on chiral dipoles

In this study, we have shown that the gain-functionalized chiral spheres can be optically sorted using single-plane waves regardless of size and particle choices. To extend the applicability of our proposal to chiral dipoles, for which only electric dipoles are prominent [53], we consider a core-shell chiral sphere with a radius of 50 nm (with an active core of 20 nm and a chiral shell of 30 nm) in Fig. 6(a) and a homogeneous chiral sphere of radius 50 nm in Fig. 6(b). Finally, we calculate

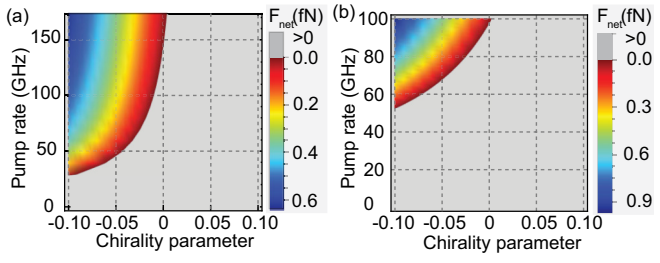

FIG. 6. (a) Density plot representing the net optical force $F_{\text{net}}(fN)$ as a function of the chirality parameter and Γ_{pump} for fixed (a) $N_{\text{dye}} = 6.4 \times 10^{18}$ cm^{-3} and (b) $N_{\text{dye}} = 0.3 \times 10^{18}$ cm^{-3}. The colored region shows the stable optical pulling force, where we have subtracted the Brownian force from the optical force.

the density plot of the stable optical pulling force ($F_{\text{net}} = F - F_B$) acting on the spheres as a function of the chirality parameter and pump power for fixed dye concentration. Thus, our approach remains valid for small particles with weak chirality.

III. CONCLUSION

In conclusion, we demonstrated an externally controllable and robust enantioselective method for single isolated chiral particles doped with gain material. By considering realistic material and geometrical parameters, we showed that this system allows one to perform enantioselection not only for lossless chiral media but also for plasmonic chiral spheres using single-plane waves. We demonstrated that by externally tuning the pump rate, a crossover between pulling and pushing force occurs for chiral shells with a given handedness, allowing for enantioselection of a racemic mixture of core-shell particles. We also demonstrated that this chiral resolution method is robust against varying the geometric parameters of the system and may be applied for arbitrarily small values of the chiral parameter, suggesting that one can also apply it to naturally occurring chiral materials.

ACKNOWLEDGMENTS

This work was supported by the São Paulo Research Foundation (FAPESP) through Grants No. 2020/03131-2, No. 2018/15580-6, No. 2018/15577-5, and No. 2018/25339-4; Coordenação de Aperfeiçoamento de Pessoal de Nível Superior - Brasil (CAPES; Finance Code 001); Conselho Nacional de Desenvolvimento Científico e Tecnológico through Grants No. 425338/2018-5 and No. 310224/2018-7; and Financiadora de Estudos e Projetos (Finep). F.A.P. acknowledges financial support from CNPq, CAPES, and FAPERJ.

The authors declare no conflicts of interest.

APPENDIX A: BROWNIAN MOTION

A sphere immersed in an aqueous solution (water in our case) must be subjected to Brownian force according to the fluctuation-dissipation theorem, which can be expressed as $F_B = \sqrt{12\pi\eta a k_\beta T}$ [54]. Here, a is the sphere radius, η is fluid viscosity, k_β is Boltzmann's constant, and T is room temperature. For the case of a subwavelength particle, say, $a = 200$ nm, immersed in water with viscosity $\eta = 7.9 \times 10^{-4}$ Pa s [54,55], the Brownian force acting on the sphere is $F_B = 5$ fN [55]. However, our results show that optical forces acting on the sphere are larger than the Brownian force even for weak incident intensity $I_0 = 1\,\text{mW}/\mu\text{m}^2$ [56]. Thus, the optical forces acting on the particle can easily overcome the thermal and Brownian fluctuations. In addition, optical forces can also be improved by increasing the power of the probing laser without changing the gain level as suggested by force expression (e.g., $F \propto I_0$).

APPENDIX B: SCATTERING OF LIGHT BY THE CHIRAL CORE-SHELL PARTICLE

Consider an electromagnetic field $\mathbf{E}_{\text{in}}$ illuminating a core-shell particle composed of a dielectric core of radius b and a chiral shell of thickness t (the outer radius $a = b + t$)

immersed in a nonmagnetic dielectric host medium of refractive index n_w. By following the Bohren decomposition method [40,43], we express the electromagnetic field in terms of the linear combinations of vector wave functions in spherical coordinates as

$$\mathbf{E}_{\text{in}} = E_0 \sum_{\ell=1}^{\infty} i^{\ell} \frac{2\ell+1}{\ell(\ell+1)} \left(M_{o1\ell}^{(1)} - iN_{e1\ell}^{(1)}\right), \tag{B1}$$

$$\mathbf{H}_{\text{in}} = H_0 \sum_{\ell=1}^{\infty} i^{\ell} \frac{2\ell+1}{\ell(\ell+1)} \left(M_{e1\ell}^{(1)} + iN_{o1\ell}^{(1)}\right), \tag{B2}$$

where $M_{e1\ell}$, $M_{o1\ell}$, $N_{e1\ell}$, and $N_{o1\ell}$ are the vector spherical harmonics [40], with $H_0 = \frac{k}{\omega\mu} E_0$. Since inside the chiral media the electric $\mathbf{E}$ and magnetic $\mathbf{H}$ fields are coupled through a phonological constant κ called the chirality parameter, the electromagnetic fields inside the media are described by the following modified constitutive relations [40]:

$$\begin{aligned} \mathbf{D} &= \epsilon_0 \epsilon_p \mathbf{E} + i\kappa \sqrt{\epsilon_0 \mu_0}\, \mathbf{H}, \\ \mathbf{B} &= -i\kappa \sqrt{\epsilon_0 \mu_0}\, \mathbf{E} + \mu_p \mu_0 \mathbf{H}, \end{aligned} \tag{B3}$$

where $\mathbf{D}$ and $\mathbf{B}$ are the electric displacement and the magnetic field, respectively. Furthermore, ϵ_0 (μ_0) is the vacuum permittivity (permeability). By using these constitutive relations in Maxwell's equations in the frequency domain, the coupling between $\mathbf{E}$ and $\mathbf{H}$ can be removed through a linear transformation [33]. In addition, the decoupling process also suggests that the wave vector k inside the chiral media is modified and can be defined as $k_{L/R} = (n_0 \pm \kappa) k_0$, where $k_0 = 2\pi/\lambda_0$ with vacuum wavelength λ_0. Finally, a straightforward calculation allows us to define the scattered field by the chiral sphere in the surrounding medium as [43,57]

$$\begin{aligned} \mathbf{E}_s &= \sum_{\ell}^{\infty} \mathcal{E}_{\ell} \left(i a_{\ell} N_{e1\ell}^3 - b_{\ell} M_{o1\ell}^3 + c_{\ell} M_{e1\ell}^3 - i d_{\ell} N_{o1\ell}^3\right), \\ \mathbf{H}_s &= \sum_{\ell}^{\infty} \mathcal{H}_{\ell} \left(a_{\ell} M_{e1\ell}^3 + i b_{\ell} N_{o1\ell}^3 - i c_{\ell} N_{e1\ell}^3 - d_{\ell} M_{o1\ell}^3\right), \end{aligned} \tag{B4}$$

where $\mathcal{E}_{\ell} = E_0 (i)^{\ell} \frac{2\ell+1}{\ell(\ell+1)}$ and $\mathcal{H}_{\ell} = H_0 (i)^{\ell} \frac{2\ell+1}{\ell(\ell+1)}$; a_{ℓ}, b_{ℓ}, c_{ℓ}, and d_{ℓ} are commonly known as Mie coefficients and can be calculated using subsidiary boundary conditions at the sphere surface. Their explicit expressions can be expressed in terms of the size parameters $\alpha = k_w b$ and $v = k_w a$, corresponding to the core and outer radii [57]. Since the shell is chiral, the refractive index of the shell can be expressed as $n_{L/R} = (\sqrt{\epsilon\mu} \pm \kappa)$, where the subscript L (R) corresponds to the left- (right-) handed polarization of the incident field. Now it is convenient to write the relative refractive indexes of the chiral shell, $N_{L/R} = (\sqrt{\epsilon\mu} \pm \kappa)/n_w$, and active core, $N_{\text{I}} = n_g/n_w$, with respect to a host medium of index n_w. Finally, $N_{\text{II}} = (N_L + N_R)/2$ is the average relative index of the chiral shell. Finally, by applying the boundary conditions we can define the unknown scattering coefficient as [57]

$$\begin{aligned} a_{\ell} &= -\Delta_{\ell}^{-1} (A_{R\ell} W_{L\ell} + A_{L\ell} W_{R\ell}), \\ b_{\ell} &= -\Delta_{\ell}^{-1} (B_{L\ell} V_{R\ell} + B_{R\ell} V_{L\ell}), \\ c_{\ell} &= i\Delta_{\ell}^{-1} (A_{L\ell} V_{R\ell} - A_{R\ell} V_{L\ell}), \\ d_{\ell} &= i\Delta_{\ell}^{-1} (B_{R\ell} W_{L\ell} - B_{L\ell} W_{R\ell}), \end{aligned}$$

with

$$\begin{aligned} \Delta_{\ell} &= W_{L\ell} V_{R\ell} + B_{L\ell} W_{R\ell}, \\ A_{R\ell} &= X_{R\ell}(-)\eta_{\ell}^{(1)}(v) - N_{\text{II}} U_{R\ell}(-) j_{\ell}(v), \\ A_{L\ell} &= X_{L\ell}(+)\eta_{\ell}^{(1)}(v) - N_{\text{II}} U_{L\ell}(+) j_{\ell}(v), \\ B_{L\ell} &= X_{L\ell}(-) N_{\text{II}} \eta_{\ell}^{(1)}(v) - U_{L\ell}(-) j_{\ell}(v), \\ B_{R\ell} &= X_{R\ell}(+) N_{\text{II}} \eta_{\ell}^{(1)}(v) - U_{R\ell}(+) j_{\ell}(v), \\ V_{L\ell} &= X_{L\ell}(+)\eta_{\ell}^{(3)}(v) - N_{\text{II}} U_{L\ell}(+) h_{\ell}^{(1)}(v), \\ V_{R\ell} &= X_{R\ell}(-)\eta_{\ell}^{(3)}(v) - N_{\text{II}} U_{R\ell}(-) h_{\ell}^{(1)}(v), \\ W_{L\ell} &= X_{L\ell}(-) N_{\text{II}} \eta_{\ell}^{(3)}(v) - U_{L\ell}(-) h_{\ell}^{(1)}(v), \\ W_{R\ell} &= X_{R\ell}(+) N_{\text{II}} \eta_{\ell}^{(3)}(v) - U_{R\ell}(+) h_{\ell}^{(1)}(v). \end{aligned}$$

We have also introduced the functions

$$\begin{aligned} X_{R\ell}(\pm) &= j_{\ell}(N_R v) + D_{4\ell} y_{\ell}(N_R v) \pm D_{2\ell} y_{\ell}(N_L v), \\ X_{L\ell}(\pm) &= j_{\ell}(N_L v) + D_{1\ell} y_{\ell}(N_L v) \pm D_{3\ell} y_{\ell}(N_R v), \\ U_{R\ell}(\pm) &= \eta_{\ell}^{(1)}(N_R v) + D_{4\ell} \eta_{\ell}^{(2)}(N_R v) \pm D_{2\ell} \eta_{\ell}^{(2)}(N_L v), \\ U_{L\ell}(\pm) &= \eta_{\ell}^{(1)}(N_L v) + D_{1\ell} \eta_{\ell}^{(2)}(N_L v) \pm D_{3\ell} \eta_{\ell}^{(2)}(N_R v), \end{aligned}$$

where

$$\begin{aligned} D_{1\ell} &= -\Delta_{\ell}^{-1} [G_{\ell}(N_R) H_{\ell}(N_L) + F_{\ell}(N_R) K_{\ell}(N_L)], \\ D_{2\ell} &= \Delta_{\ell}^{-1} [F_{\ell}(N_R) K_{\ell}(N_R) - G_{\ell}(N_R) H_{\ell}(N_R)], \\ D_{3\ell} &= \Delta_{\ell}^{-1} [G_{\ell}(N_L) H_{\ell}(N_L) - F_{\ell}(N_L) K_{\ell}(N_L)], \\ D_{4\ell} &= -\Delta_{\ell}^{-1} [G_{\ell}(N_L) H_{\ell}(N_R) + F_{\ell}(N_L) K_{\ell}(N_R)]. \end{aligned}$$

F, G, H, and K are functions of the refractive index variable $N = N_L, N_R$, defined as

$$\begin{aligned} F_{\ell}(N) &= N_{\text{II}} y_{\ell}(N\alpha) \eta_{\ell}^{(1)}(N_{\text{I}}\alpha) - N_{\text{I}} \eta_{\ell}^{(2)}(N\alpha) j_{\ell}(N_{\text{I}}\alpha), \\ G_{\ell}(N) &= N_{\text{I}} y_{\ell}(N\alpha) \eta_{\ell}^{(1)}(N_{\text{I}}\alpha) - N_{\text{II}} \eta_{\ell}^{(2)}(N\alpha) j_{\ell}(N_{\text{I}}\alpha), \\ H_{\ell}(N) &= N_{\text{I}} j_{\ell}(N\alpha) \eta_{\ell}^{(1)}(N_{\text{I}}\alpha) - N_{\text{I}} \eta_{\ell}^{(1)}(N\alpha) j_{\ell}(N_{\text{I}}\alpha), \\ K_{\ell}(N) &= N_{\text{II}} j_{\ell}(N\alpha) \eta_{\ell}^{(1)}(N_{\text{I}}\alpha) - N_{\text{II}} \eta_{\ell}^{(1)}(N\alpha) j_{\ell}(N_{\text{I}}\alpha). \end{aligned}$$

$j_{\ell}(\rho)$ and $y_{\ell}(\rho)$ are the spherical Bessel functions of the first and second kinds, respectively, and $h_{\ell}^{(1)}(\rho)$ is the spherical Hankel function of the first kind. We also define

$$\begin{aligned} \eta_{\ell}^{(1)}(\rho) &= \frac{1}{\rho} d[\rho j_{\ell}(\rho)]/d\rho, \\ \eta_{\ell}^{(2)}(\rho) &= \frac{1}{\rho} d[\rho y_{\ell}(\rho)]/d\rho, \\ \eta_{\ell}^{(3)}(\rho) &= \frac{1}{\rho} d[\rho h_{\ell}^{(1)}(\rho)]/d\rho. \end{aligned}$$

For the sake of convenience, we can define the effective scattering coefficients which are the perfect analog of the Mie scattering coefficients of a conventional dielectric sphere [22] as $A_{\ell} = a_{\ell} + i\sigma c_{\ell}$ and $B_{\ell} = b_{\ell} - i\sigma d_{\ell}$ for circularly polarized light of helicity σ.

With the help of these scattering coefficients, we can quantify the energy received and scattered by the sphere in terms of the extinction cross section C_{ext} and the scattering cross section C_s, respectively. To get rid of the units involved in

the cross sections, we define the dimensionless efficiency Q by dividing the geometric cross section of the sphere as $Q_j = C_j/\pi a^2$ ($j = \text{ext}, s$):

$$Q_{\text{ext}} = C_{\text{ext}}/\pi a^2 = \frac{2}{x^2}\sum_{\ell=1}^{\infty}(2\ell+1)\text{Re}(A_\ell + B_\ell), \tag{B5}$$

$$Q_s = C_s/\pi a^2 = \frac{2}{x^2}\sum_{\ell=1}^{\infty}(2\ell+1)(|A_\ell|^2 + |B_\ell|^2), \tag{B6}$$

where $x = k_w a$. Since we have an active core that provides photon emission being controlled by an external source [see Fig. 1(b)], the energy received by the probing laser and the energy scattered by the sphere are different and depend on several parameters, as discussed in the main text. Thus, it is convenient to define the negative absorption or gain efficiency [40,58,59] as

$$Q_a = Q_{\text{ext}} - Q_s. \tag{B7}$$

It is worth mentioning that the sign of Q_a is controlled by controlling the sign of the imaginary refractive index of the media. For instance, Q_a is negative for $\text{Im}(m) < 0$, corresponding to gain media, and Q_a is positive for $\text{Im}(m) > 0$, corresponding to lossy media, under the $\exp^{-i\omega t}$ convention.

APPENDIX C: RADIATION PRESSURE DUE TO A PLANE WAVE

Light carries momentum that can be transferred to a particle; therefore, a beam that interacts with a particle exerts a radiation force. If we consider that a light beam consists of a stream of photons, it is physically reasonable to assert that the photons absorbed by the particle transfer all their momentum to the particle and exert force in the propagation direction. In contrast, the photons scattered by the sphere exert force in the direction opposite of the scattering direction defined by the scattering angle θ. Therefore, the net force on the particle can be defined in terms of extinction efficiency (Q_{ext} denotes the energy received by the particle), scattering efficiency (Q_s denotes the energy scattered by the particle), and the asymmetry parameter ($\langle\cos\theta\rangle$ denotes the scattering direction) as [40]

$$F = \frac{\epsilon_0\epsilon_w E_0^2}{k_w^2}(Q_{\text{ext}} - Q_s\langle\cos\theta\rangle), \tag{C1}$$

where E_0^2 is the amplitude of the incident field, which can be associated with the incident-field intensity as $I_0 = c\epsilon_0 E_0^2/2$, and $\langle\cos\theta\rangle$ is the asymmetric parameter with scattering angle θ and is given as [40]

$$\langle\cos\theta\rangle = \frac{4}{Q_s x^2}\left(\sum_{\ell=1}^{\infty}\frac{\ell(\ell+2)}{\ell+1}\text{Re}(A_\ell A_{\ell+1}^* + B_\ell B_{\ell+1}^*) + \sum_{\ell=1}^{\infty}\frac{2\ell+1}{\ell(\ell+1)}\text{Re}(A_\ell B_\ell^*)\right). \tag{C2}$$

For a passive sphere $Q_{\text{ext}} \geqslant Q_s$, it is clear that for a particle with zero backscattering (with $\langle\cos\theta\rangle = 1$) the sphere will experience $F \geqslant 0$, which should always be pushing.

Since we have an active core and $Q_{\text{ext}} \neq Q_s$, it is worth explicitly discussing the force due to the emission of the photons. The force now can be expressed as

$$F = \frac{\epsilon_0\epsilon_w E_0^2}{k_w^2}[Q_{\text{a}} + Q_{\text{s}}(1 - \langle\cos\theta\rangle)] = F_{\text{a}} + F_{\text{s}}, \tag{C3}$$

where F_a and F_s are the force contributions due to the emission of the photons (which is toward the source) and the scattering of the photons (in the propagation direction), respectively.

[1] G. H. Wagnièree, *On Chirality and the Universal Asymmetry: Reflections on Image and Mirror Image* (VHCA, Zürich, 2007).

[2] M. Hentschel, M. Schäferling, X. Duan, H. Giessen, and N. Liu, Chiral plasmonics, Sci. Adv. **3**, e1602735 (2017).

[3] Z. Fan and A. O. Govorov, Plasmonic circular dichroism of chiral metal nanoparticle assemblies, Nano Lett. **10**, 2580 (2010).

[4] A. Kuzyk, R. Schreiber, Z. Fan, G. Pardatscher, E.-M. Roller, A. Högele, F. C. Simmel, A. O. Govorov, and T. Liedl, DNA-based self-assembly of chiral plasmonic nanostructures with tailored optical response, Nature (London) **483**, 311 (2012).

[5] J. Zhang, M. T. Albelda, Y. Liu, and J. W. Canary, Chiral nanotechnology, Chirality **17**, 404 (2005).

[6] W. H. Brooks, W. C. Guida and K. G. Daniel, The significance of chirality in drug design and development, Curr. Top. Med. Chem. **11**, 760 (2011).

[7] M. J. Urban, C. Shen, X.-T. Kong, C. Zhu, A. O. Govorov, Q. Wang, M. Hentschel, and N. Liu, Chiral plasmonic nanostructures enabled by bottom-up approaches, Annu. Rev. Phys. Chem. **70**, 275 (2019).

[8] Y. Zhao, A. A. E. Saleh, and J. A. Dionne, Enantioselective optical trapping of chiral nanoparticles with plasmonic tweezers, ACS Photon. **3**, 304 (2016).

[9] Y. Zhao, A. A. E. Saleh, M. A. van de Haar, B. Baum, J. A. Briggs, A. Lay, O. A. Reyes-Becerra, and J. A. Dionne, Nanoscopic control and quantification of enantioselective optical forces, Nat. Nanotechnol. **12**, 1055 (2017).

[10] G. Tkachenko and E. Brasselet, Optofluidic sorting of material chirality by chiral light, Nat. Commun. **5**, 3577 (2014).

[11] R. Ali and Y. Wu, Enantioselective transport of chiral spheres using focused femtosecond laser pulses, Opt. Express **31**, 29716 (2023).

[12] S. B. Wang and C. T. Chan, Lateral optical force on chiral particles near a surface, Nat. Commun. **5**, 3307 (2014).

[13] H. Chen, C. Liang, S. Liu, and Z. Lin, Chirality sorting using two-wave-interference–induced lateral optical force, Phys. Rev. A **93**, 053833 (2016).

[14] T. Zhang, M. R. C. Mahdy, Y. Liu, J. H. Teng, C. T. Lim, Z. Wang, and C.-W. Qiu, All-optical chirality-sensitive sorting via reversible lateral forces in interference fields, ACS Nano **11**, 4292 (2017).

[15] Y. Q. Wang, H. Hu, Q. Zhang, D. L. Gao, and L. Gao, Topologically-tuned spin Hall shift around Fano resonance, Opt. Express **28**, 21641 (2020).

[16] H. Wu, P. Zhang, X. Zhang, Y. Hu, Z. Chen, and J. Xu, Selective trapping of chiral nanoparticles via vector Lissajous beams, Opt. Express **30**, 3592 (2022).
[17] H. Chen, N. Wang, W. Lu, S. Liu, and Z. Lin, Tailoring azimuthal optical force on lossy chiral particles in Bessel beams, Phys. Rev. A **90**, 043850 (2014).
[18] C. Genet, Chiral light–chiral matter interactions: An optical force perspective, ACS Photon. **9**, 319 (2022).
[19] A. Hayat, J. P. B. Mueller, and F. Capasso, Lateral chirality-sorting optical forces, Proc. Natl. Acad. Sci. USA **112**, 13190 (2015).
[20] R. Ali, R. S. Dutra, F. A. Pinheiro, and P. A. M. Neto, Enantioselection and chiral sorting of single microspheres using optical pulling forces, Opt. Lett. **46**, 1640 (2021).
[21] H. Zheng, X. Li, H. Chen, and Z. Lin, Selective transport of chiral particles by optical pulling forces, Opt. Express **29**, 42684 (2021).
[22] R. Ali, F. A. Pinheiro, R. S. Dutra, F. S. S. Rosa, and P. A. Maia Neto, Enantioselective manipulation of single chiral nanoparticles using optical tweezers, Nanoscale **12**, 5031 (2020).
[23] M. Li, S. Yan, Y. Zhang, X. Chen, and B. Yao, Optical separation and discrimination of chiral particles by vector beams with orbital angular momentum, Nanoscale Adv. **3**, 6897 (2021).
[24] A. Canaguier-Durand, J. A. Hutchison, C. Genet, and T. W. Ebbesen, Mechanical separation of chiral dipoles by chiral light, New J. Phys. **15**, 123037 (2013).
[25] K. Ding, J. Ng, L. Zhou, and C. T. Chan, Realization of optical pulling forces using chirality, Phys. Rev. A **89**, 063825 (2014).
[26] A. Canaguier-Durand and C. Genet, Chiral route to pulling optical forces and left-handed optical torques, Phys. Rev. A **92**, 043823 (2015).
[27] N. Kravets, A. Aleksanyan, and E. Brasselet, Chiral optical stern-gerlach Newtonian experiment, Phys. Rev. Lett. **122**, 024301 (2019).
[28] G. Tkachenko and E. Brasselet, Helicity-dependent three-dimensional optical trapping of chiral microparticles, Nat. Commun. **5**, 4491 (2014).
[29] F. Patti, R. Saija, P. Denti, G. Pellegrini, P. Biagioni, M. A. Iatì, and O. M. Maragò, Chiral optical tweezers for optically active particles in the T-matrix formalism, Sci. Rep. **9**, 29 (2019).
[30] D. S. Bradshaw and D. L. Andrews, Chiral discrimination in optical trapping and manipulation, New J. Phys. **16**, 103021 (2014).
[31] R. J. Hernández, A. Mazzulla, A. Pane, K. Volke-Sepúlveda, and G. Cipparrone, Attractive-repulsive dynamics on light-responsive chiral microparticles induced by polarized tweezers, Lab Chip **13**, 459 (2013).
[32] R. Ali, F. A. Pinheiro, R. S. Dutra, F. S. S. Rosa, and P. A. M. Neto, Probing the optical chiral response of single nanoparticles with optical tweezers, J. Opt. Soc. Am. B **37**, 2796 (2020).
[33] R. Ali, R. S. Dutra, F. A. Pinheiro, F. S. S. Rosa, and P. A. Maia Neto, Theory of optical tweezing of dielectric microspheres in chiral host media and its applications, Sci. Rep. **10**, 16481 (2020).
[34] J. Chen, J. Ng, Z. Lin, and C. T. Chan, Optical pulling force, Nat. Photon. **5**, 531 (2011).
[35] Z. Fan and A. O. Govorov, Chiral nanocrystals: Plasmonic spectra and circular dichroism, Nano Lett. **12**, 3283 (2012).
[36] J. E. Lu, C.-H. Yang, H. Wang, C. Yam, Z.-G. Yu, and S. Chen, Plasmonic circular dichroism of vesicle-like nanostructures by the template-less self-assembly of achiral Janus nanoparticles, Nanoscale **10**, 14586 (2018).
[37] C. Rao, Z.-G. Wang, N. Li, W. Zhang, X. Xu, and B. Ding, Tunable optical activity of plasmonic dimers assembled by DNA origami, Nanoscale **7**, 9147 (2015).
[38] X. Lan and Q. Wang, Self-assembly of chiral plasmonic nanostructures, Adv. Mater. **28**, 10499 (2016).
[39] G. Cipparrone, A. Mazzulla, A. Pane, R. J. Hernandez, and R. Bartolino, Chiral self-assembled solid microspheres: A novel multifunctional microphotonic device, Adv. Mater. **23**, 5773 (2011).
[40] C. F. Bohren and D. R. Huffman, *Absorption and scattering of light by small particles* (Wiley, New York, 1998), Chap. 4, pp. 83–122.
[41] A. Mizrahi and Y. Fainman, Negative radiation pressure on gain medium structures, Opt. Lett. **35**, 3405 (2010).
[42] T. Kudo and H. Ishihara, Proposed nonlinear resonance laser technique for manipulating nanoparticles, Phys. Rev. Lett. **109**, 087402 (2012).
[43] C. F. Bohren and D. R. Huffman, *Absorption and scattering of light by small particles* (Wiley, New York, 1998), Chap. 8, pp. 182–223.
[44] L. Pezzi, M. A. Iatì, R. Saija, A. De Luca, and O. M. Maragò, Resonant coupling and gain singularities in metal/dielectric multishells: Quasi-static versus T-matrix calculations, J. Phys. Chem. C **123**, 29291 (2019).
[45] P. Polimeno, F. Patti, M. Infusino, J. Sánchez, M. A. Iatì, R. Saija, G. Volpe, O. M. Maragò, and A. Veltri, Gain-assisted optomechanical position locking of metal/dielectric nanoshells in optical potentials, ACS Photon. **7**, 1262 (2020).
[46] S. Campione, M. Albani, and F. Capolino, Complex modes and near-zero permittivity in 3D arrays of plasmonic nanoshells: Loss compensation using gain [Invited], Opt. Mater. Express **1**, 1077 (2011).
[47] H. Doan, M. Castillo, M. Bejjani, Z. Nurekeyev, S. V. Dzyuba, I. Gryczynski, Z. Gryczynski, and S. Raut, Solvatochromic dye LDS 798 as microviscosity and pH probe, Phys. Chem. Chem. Phys. **19**, 29934 (2017).
[48] R. Ali, Tunable anomalous scattering and negative asymmetry parameter in a gain-functionalized low refractive index sphere, ACS Omega **7**, 2170 (2022).
[49] Y. Shi, L.-M. Zhou, A. Q. Liu, M. Nieto-Vesperinas, T. Zhu, A. Hassanfiroozi, J. Liu, H. Zhang, D. P. Tsai, H. Li, W. Ding, W. Zhu, Y. F. Yu, A. Mazzulla, G. Cipparrone, P. C. Wu, C. T. Chan, and C.-W. Qiu, Superhybrid mode-enhanced optical torques on Mie-resonant particles, Nano Lett. **22**, 1769 (2022).
[50] R. Ali, R. S. Dutra, F. A. Pinheiro, and P. A. M. Neto, Gain-assisted optical tweezing of plasmonic and large refractive index microspheres, J. Opt. **23**, 115004 (2021).
[51] F. Chen, J. Wang, C. Ye, W. Ni, J. Chan, Y. Yang, and D. Lo, Near infrared distributed feedback lasers based on LDS dye-doped zirconia-organically modified silicate channel waveguides, Opt. Express **13**, 1643 (2005).
[52] N. Cathcart and V. Kitaev, Monodisperse hexagonal silver nanoprisms: Synthesis via thiolate-protected cluster precursors and chiral, ligand-imprinted self-assembly, ACS Nano **5**, 7411 (2011).
[53] R. Ali, F. A. Pinheiro, R. S. Dutra, and P. A. Maia Neto, Tailoring optical pulling forces with composite microspheres, Phys. Rev. A **102**, 023514 (2020).

[54] K. Okamoto and S. Kawata, Radiation force exerted on subwavelength particles near a nanoaperture, Phys. Rev. Lett. **83**, 4534 (1999).

[55] M. Li, S. Yan, B. Yao, Y. Liang, G. Han, and P. Zhang, Optical trapping force and torque on spheroidal Rayleigh particles with arbitrary spatial orientations, J. Opt. Soc. Am. A **33**, 1341 (2016).

[56] O. Brzobohatý, V. Karásek, M. Šiler, L. Chvátal, T. Čižmár, and P. Zemánek, Experimental demonstration of optical transport, sorting and self-arrangement using a 'tractor beam,' Nat. Photon. **7**, 123 (2013).

[57] C. F. Bohren, Scattering of electromagnetic waves by an optically active spherical shell, J. Chem. Phys. **62**, 1566 (1975).

[58] P. L. Marston and J. H. Crichton, Radiation torque on a sphere caused by a circularly-polarized electromagnetic wave, Phys. Rev. A **30**, 2508 (1984).

[59] C. F. Bohren, Radiation forces and torques without stress (tensors), Eur. J. Phys. **32**, 1515 (2011).